processes

MDPI

Article

Thermodynamic Modeling of a Solar-Driven Organic Rankine Cycle-Absorption Cooling System for Simultaneous Power and Cooling Production

José C. Jiménez-García [1], Isaías Moreno-Cruz [2] and Wilfrido Rivera [1,*]

[1] Instituto de Energías Renovables, Universidad Nacional Autónoma de México, Temixco 62580, Mexico; jcjig@ier.unam.mx
[2] Laboratorio de Energía Solar Térmica, Centro de Investigaciones en Óptica AC, Aguascalientes 20200, Mexico; ismoc@cio.mx
* Correspondence: wrgf@ier.unam.mx

Abstract: Humanity is facing the challenge of reducing its environmental impact. For this reason, many specialists worldwide have been studying the processes of production and efficient use of energy. In this way, developing cleaner and more efficient energy systems is fundamental for sustainable development. The present work analyzed the technical feasibility of a solar-driven power-cooling system operating in a particular location in Mexico. The theoretical system integrates organic Rankine and single-stage absorption cooling cycles. A parabolic trough collector and a storage system integrated the solar system. Its performance was modeled for a typical meteorological year using the SAM software by NREL. The analyzed working fluids for the organic cycle include benzene, cyclohexane, toluene, and R123, while the working fluid of the absorption system is the ammonia-water mixture. The cycle's first and second-law performances are determined in a wide range of operating conditions. Parameters such as the energy utilization factor, turbine power, COP, and exergy efficiency are reported for diverse operating conditions. It was found that the highest energy utilization factor was 0.68 when the ORC utilized benzene as working fluid at ORC and ACS condensing temperatures of 80 °C and 20 °C, respectively, and at a cooling temperature of 0 °C. The best exergy efficiency was 0.524 at the same operating conditions but at a cooling temperature of −10 °C.

Keywords: solar energy; organic Rankine cycle; absorption system; solar cooling and power; parabolic trough

Citation: Jiménez-García, J.C.; Moreno-Cruz, I.; Rivera, W. Thermodynamic Modeling of a Solar-Driven Organic Rankine Cycle-Absorption Cooling System for Simultaneous Power and Cooling Production. *Processes* **2024**, *12*, 427. https://doi.org/10.3390/pr12030427

Academic Editors: Mateo Bašić and Dejan Jokić

Received: 22 January 2024
Revised: 15 February 2024
Accepted: 16 February 2024
Published: 20 February 2024

1. Introduction

One of the main consequences of the irrational use of energy systems, mainly of those with direct or indirect use of fossil fuels, is climate change, whose effects on the planet have been studied in recent decades and today are well known. In the last decades, a strategy well promoted to counteract such effects is the transition to systems using renewable energy sources, such as solar energy, which can be used to produce electricity through the well-known photovoltaic technologies, or heat through the different solar thermal devices. These energy sources are of interest to the present research work.

1.1. Solar-Thermal Energy Technologies

In recent years, the research and development of solar technologies have not only enhanced the efficiencies of diverse systems but have also made significant strides in improving thermal energy storage and distribution, as well as the overall design, monitoring, control, and integration of these systems. Diverse solar technologies offer versatile applications, capitalizing on one of the most popular renewable energy sources.

Solar thermal energy is practical in diverse applications such as water and space heating, cooking, drying, desalination, distillation, industrial processes, thermal power gen-

eration, cooling and air conditioning, thermal energy storage, thermal hybrid systems, and steam generation. Notably, thermal power generation has garnered substantial attention from researchers in recent decades due to the environmental impact, particularly the contribution to global warming, associated with fossil fuels commonly used in thermoelectric power plants (often relying on natural gas or coal).

According to the 2021 Statistical Review of World Energy [1], coal and natural gas dominated power generation, contributing 36% and 22.9% to total production, respectively. While renewable energy sources, including wind and solar, have made strides, their combined contribution to global electricity production was reported at 10.2% for the same year. Some experts suggest directing research efforts toward expanding solar power applications, particularly in electricity generation, to reduce dependency on conventional grids [2].

1.2. Organic Rankine Cycles (ORCs)

Regarding power production using alternative energy sources instead of fossil fuels, a very popular system that has gained the attention of researchers in that field is the organic Rankine cycle (ORC) since it offers several advantages over the conventional Rankine cycle, the main one being that it can use low and medium-temperature heat sources which could not be used by a conventional Rankine cycle since it requires higher operation temperatures [3]. Thus, the ORC is interesting, mainly when used for waste heat recovery, low-temperature heat sources, and applications where water as a working fluid is not feasible. Other key advantages of the ORC compared to the traditional Rankine cycle are described next:

- A wider range of working fluids. Such flexibility enables the optimization of the cycle for specific heat source temperatures. Recent research on organic fluids has addressed issues like their thermodynamic performance [4], actual greenhouse effect [5,6], the use of zeotropic mixtures as working fluids [7–11], and the effect of using super dry working fluids on system performance [12,13].
- A more compact design. ORCs require lower operating pressures and, thus, smaller equipment sizes than conventional Rankine cycles. This advantage can lead to more compact and cheaper system designs. This advantage is particularly convenient for limited-space applications.
- Customizable systems: ORCs can be customized and optimized for specific applications and heat source conditions. This flexibility allows engineers to design systems that match the requirements of the particular energy source [3,14–16] and heat sink, maximizing efficiency [3,14–20].
- Modular and Scalable: ORC systems are often modular and can be scaled to suit different power output requirements. This characteristic makes them suitable for various applications, from small-scale distributed power generation to large industrial processes.
- Decentralized Power Generation: ORCs are suitable for decentralized power generation, enabling the utilization of local heat sources to produce electricity. This can improve energy efficiency and reduce transmission losses.
- Combined Heat and Power (CHP) Systems: ORCs can be integrated into combined heat and power systems, allowing the simultaneous generation of electricity and useful heat and increasing the overall energy utilization efficiency. New researchs on combined heat and power systems have utilized ORC, taking advantage of several heat sources [21–25].

It is important to note that these cycles also come with their challenges and considerations, such as the choice of the working fluid, thermodynamic cycle design, equipment compatibility, and safety concerns associated with some organic fluids; despite this, their versatility and advantages make of them one of the main options to consider for power production when there are low or medium temperature heat sources.

1.3. Absorption Cooling Systems (ACS)

On the other hand, it is well known that vapor compression cooling systems are the most utilized systems worldwide for cooling purposes. However, they have direct and indirect negative impacts on the environment due to direct emissions of some refrigerants with Ozone Depletion Potential (ODP) and their use of electricity produced mainly by fossil fuels, indirectly contributing to global warming [26]. Moreover, according to some prospects [27], the cooling demand in the next decades will increase so that only the contribution of cooling systems to global warming will surpass the limit aimed for in the Paris Agreement. Thus, it is necessary to focus on actions aiming to create efficient and reliable alternative cooling systems capable of satisfying increasing cooling demand in the future. An alternative to conventional compression systems is absorption systems, which have gained attention in the last decades since they can be operated with a heat source, reducing (or even avoiding) the dependence on electricity to produce a cooling effect. In general, the research on absorption cooling systems seeks an improvement in efficiency, sustainability, and applicability. To achieve that, recent research has focused on topics such as the following:

- Advanced absorbent materials: Researchers are investigating new materials to enhance vapor capture and release efficiency in absorption cycles. These new materials could lead to more efficient and lower-energy consumption cooling systems. Some of these absorbents are ionic liquids [28–30], although other fluids have been studied [31].
- Cycle Efficiency Enhancement: Different techniques to optimize and enhance absorption cycles are being explored to reduce heat losses and improve mass transfer during absorption and desorption processes [32].
- Renewable Energy Integration: Researchers are exploring ways to integrate absorption systems with renewable energy sources such as solar or geothermal energy to make cooling systems more sustainable and self-sufficient [33–37].
- Hybrid Systems: Absorption systems integrated with other cooling technologies, such as mechanical compression systems, have been investigated to achieve optimal performance and higher energy efficiency [38,39].

1.4. Integrated Cooling and Power Systems

According to the report "The Cooling Imperative: Forecasting the Size and Source of Future Cooling Demand" [27], it was estimated that 470 million people in poor rural areas lack access to safe food and medicines due to inadequate electricity and refrigeration. In this context, hybrid systems for the simultaneous production of power and cooling could be an effective way to satisfy these two elemental needs at once. For this purpose, integrating organic Rankine cycles and absorption cooling systems is very attractive because of the advantages previously described for every system. Moreover, hybrid systems driven by solar energy for power and cooling could satisfy these basic needs where no grid access is available. In such cases, its energetic and economic performance could reach attractive values because of its high potential for an off-grid operation.

Research on hybrid systems for power and cooling has been intensified in the last few years. Most of this research is the result of modifications to basic power cycles (i.e., Rankine and Kalina cycles) and their integration into a cooling cycle, which, for convenience, turns out to be the absorption cycle. From that point, some cycles are continuously modified to get more complex systems to produce more than two energy effects. Some representative examples of the research on integrated systems are briefly described in the next paragraphs.

One of the most known cycles for simultaneous cooling and power production is the Goswami cycle [40], which combines absorption and a Rankine cycle with power production as the primary goal. The working fluid in this cycle is the ammonia–water mixture, which, according to the authors, is ideally suited for solar thermal power using low-cost solar concentrating collectors. The Goswami cycle has been extensively studied [41–44] because of its high versatility for using different heat sources, including those at low and medium temperatures. Some studies have been performed based on the Goswami cycle.

Hasan and Goswami analyzed the Goswami cycle operated with solar energy from the second law perspective [45]. The analysis considered optimizing the operating conditions to get maximum exergy efficiency. Heat source temperatures from 47 to 187 °C were considered in the analysis. The authors found that increasing the heat source temperature does not necessarily increase the energy or exergy efficiencies. However, it was proved that the heat source temperature affects the fractions of power and refrigeration. Another study [46] theoretically analyzed several configurations for simultaneous cooling and power production using absorption systems with working fluids based on ammonia. This study considered different configurations based on the Goswami and single-effect absorption cycles coupled to several solar collectors (evacuated tube, parabolic trough, and linear Fresnel). This study found an optimum heat source temperature for each configuration depending on the solar technology, the evacuated tube solar collector being the most suitable for single-effect configurations since the temperature requirement is low. However, for applications requiring a higher heat source temperature, as the Goswami cycle does, the authors found that the parabolic trough collector could be a good option.

Other studies for the simultaneous production of power and cooling have been focused on the integration of organic Rankine cycles (ORC) and cooling systems such as vapor compression refrigeration cycles (VCRC), ejector refrigeration cycles (ERC), and absorption cooling systems (ACS).

Regarding the studies integrating an ORC and a VCRC, Alshammari et al. [47] modeled and experimentally validated a new single-rotor expander-compressor device in a combined VCRC and ORC. The system was analyzed at a driven temperature of 90 °C, evaporator temperatures in the VCRC between −20 °C and −5 °C, and rotor speed (500–3000 rpm). The maximum cooling effect, heat-to-cooling efficiency, and exergy efficiency achieved were 5.38 kW, 56%, and 63%, respectively, at evaporator temperatures of 62.75 °C for the ORC and −5 °C for the VCRC. Kim [48] modeled a combined power generation and cooling system comprising an ORC and a VCRC using R245fa, R114, R600, R142b, R152a, and R1234yf. The results showed that the thermal efficiency of the combined ORC–VCC system was almost twice that of the basic ORC system. The results showed that the R245fa exhibited the highest thermal efficiency of 25%, which was 29% higher than the 19.4% achieved using R1234yf under the same operating conditions. Grauberger et al. [49] designed and evaluated an experimental ORC–VCRC of 300 kWth using novel heat integration strategies. The system uses a turbo-compressor sharing a single shaft. The system operated with waste heat at 91 °C and generated chilled water at 7 °C. The thermal efficiency of the Rankine cycle (accounting for pump work) was 7.7%, and the COP of the VCRC was 5.25. Nasir et al. [50] analyzed a biomass-powered combined cooling, heating, and power system based on ORC and VCRC for small-scale developing and underdeveloped communities. The ORC operated with xylene and could deliver 100 kW of electricity. Meanwhile, isobutane was used in the VCRC. The system delivered as much as 30 kW of cooling and 528 kW of heating at various combinations of parameters.

Concerning the integration of an ORC with an ERC, Gorhbani et al. [51] proposed a cogeneration system to produce cooling, heating, and power from geothermal energy. The cogeneration system comprises a Kalina cycle (KC), an ERC, and an ORC. The authors conducted energy, exergy, and exergoeconomic analyses with a multi-objective optimization. Thermal efficiency, exergy efficiency, total investment cost, total exergy destruction rate, net power production capacity, and cycle cooling capacity at optimal conditions were 23.04%, 26.55%, 45,944.5 $/yr, 226 kW, 75.17 kW, and 111.6 kW, respectively. Tao et al. [52] analyzed and optimized a combined power and refrigeration system based on ORC and ERC. The evaporation temperature was as low as −60 °C. The system was compared with others reported in the literature, finding that under the same operating conditions, the system's net power was increased by 12.52 kW, the thermal efficiency was increased by 4.27%, and the energy efficiency was increased by 2.57%. The optimum system thermal efficiency, the exergy efficiency, the sum unit cost of products, and the sum unit environmental products were 15.01%, 43.18%, 45.5 USD/MWh, and 5122.6 MPTS/MWh, respectively. Chowdhury

and Mokheimer [53] analyzed the performance of a combined power and cooling cycle consisting of an ORC and an ejector absorption refrigeration cycle. The ORC was modeled with different working fluids, while the refrigeration cycle operated with the ammonia–lithium nitrate mixture. Parabolic trough collectors drove the whole system. The modeling results showed that the PTC accounted for 60–80% of the total exergy destruction. The highest energy utilization factor was 25.31% at a fluid inlet temperature of 550 K, using toluene as a working fluid in the ORC. The highest exergy efficiency was 17%.

Regarding the systems integrating an ORC and an ACS, Liu et al. [54] analyzed a system integrated by two ORCs (one of them of multiple stages), a compressed air energy storage, and an ACS to produce heating, cooling, and power simultaneously. The optimization was performed using *Aspen Plus* software to maximize the round-trip efficiency and minimize the total investment cost per output power. The results showed that the system has the advantages of a high efficiency of 68.38% and a low cost of 0.1984 $/kWh. Sharifishourabi and Chadegani [55] studied a system for the production of hydrogen, cooling, hot water, and power through the integration of an organic cycle, a triple-effect absorption cooling system, a dehumidifier, and an electrolyzer using a compound parabolic trough solar collector. In the proposed system, the power output was used to activate the electrolyzer and produce hydrogen, while the organic fluid at the turbine outlet was used to activate the cooling system. The performance parameters achieved by the system were 0.39, 1.34, and 14.4% for the energy utilization factor, the COP of the cooling system, and energy efficiency, respectively. Anvari et al. [56] proposed and analyzed a trigeneration system consisting of a gas-turbine cycle, a heat-recovery steam generator, and an absorption cycle operating with the H_2O–LiBr to produce a combined cooling, heating, and power. The proposed configuration capacity can generate a power of 30 MW, 40 MW of heating, and 2 MW of cooling. The authors found that the combustion chamber had the highest contribution to the overall exergy destruction and that nearly 29% of the total irreversibility in the cycle was endogenous-avoidable. From the second-law perspective, Pashapour et al. [57] analyzed a polygeneration system for heating, cooling, and power. The proposed system integrated a gas turbine, an ORC, and an ACS. The system uses the heat lost from a gas turbine to drive the organic cycle and, at the same time, to produce warm water. Geothermal heat is used in a reheater in the organic cycle to improve the power produced (achieving an increase of 29.4% regarding the non-reheating cycle) and then to drive the absorption cycle for cooling production. It was found that a maximum exergy efficiency of 50.65% was achieved. Jiménez et al. [58] analyzed the coupling of an organic cycle and an absorption cooling system using different organic fluids. The authors found that power output is, at best, one-quarter of the cooling output for a wide range of operative conditions. This is because the expansion of the organic fluid in the power cycle is limited by the need to obtain a fluid at a high temperature at the outlet of the expander to activate the double-effect absorption cycle. The energy utilization factor and the exergy efficiency varied between 0.62 and 0.76, and 0.14 and 0.35, respectively. Grosu et al. [59] integrated an ORC using R245fa and an H_2O–LiBr ACS driven by solar energy. It was designed to supply electricity and air conditioning to a building; however, this study mainly focused on the organic and absorption cycles, leaving aside the solar system details. The authors recommend adding a recovery heat exchanger at the inlet of the condenser in the ORC and including a solution heat exchanger in the absorption cycle to improve the efficiency of the integrated system.

Additionally, Gupta et al. [60] reviewed a solar ORC and its polygeneration applications. The authors reported 160 references to systems related to the topic, most of which analyzed systems for the production of electricity and heating, electricity, heating and cooling, electricity, heating, and freshwater, among other applications. Regarding the systems studied for electricity and cooling, in almost all cases, the systems were integrated using an ORC and a VCRC, while just a couple of them used absorption systems; however, in both cases, the absorption systems were not used for cooling production but for heating or fresh water.

From the literature reviewed, it is clear that there have been many studies of ORC driven with solar energy [60] for a wide range of applications. Also, many studies have been reported for the simultaneous production of power and cooling, but most of these studies integrate a VCRC into an ORC [47,49,50]. Also, many systems have used an ERC for cooling purposes [51–53]. Only a few studies have integrated an ACS for cooling production [54–57], and in fact, just the system analyzed by Grosu et al. [59] was driven by solar energy. Thus, it is clear that there is a lack of studies integrating ORC and ACS for the simultaneous production of power and cooling driven by solar energy. Additionally, it was observed that, in all the cases in which an ACS was integrated into an ORC, the ACS operated with the H_2O–LiBr mixture, thus limiting their applications just for air conditioning without the possibility of producing cooling under 0 °C. Therefore, the present study proposes and analyzes the theoretical performance of an integrated organic Rankine cycle/single-effect absorption cooling system (ORC–ACS) driven by a solar system composed of a commercial Parabolic Trough Solar Collector (PTSC) coupled to thermal storage. For that purpose, the analysis considered the solar conditions available in Temixco, Morelos, Mexico. The solar analysis was carried out using the NREL System Advisor Model (SAM 2022.11.21 version) software [61], whose output values for thermal load and temperature (delivered by the solar system) characterize the thermal input to the integrated cooling and power system. Thus, the cooling and power production will be assessed under the specified conditions.

As for the working fluids selection, the proposed fluids for the system are benzene, toluene, cyclohexane, and R123 for the ORC and the ammonia–water (NH_3–H_2O) mixture for the ACS. The choice of the organic fluids was based on previous reports [4,62–64], where the best efficiencies for the organic Rankine cycles operated in similar conditions to those of the present study were obtained with benzene, toluene, and cyclohexane. As for the selection of R123, it was influenced by several recommendations in the literature [65–68], mainly considering the thermodynamic and environmental performances achieved. The organic fluids chosen are dry fluids suitable for the ORC operation. Some relevant properties of these fluids are presented in Table 1.

Table 1. Selected organic fluids' properties.

Fluid	Critical Temperature (°C)	Temperature on Turning Point (°C)	ORC Thermal Efficiency	ODP	GWP
Benzene	288.9	263.35	28.92	0	Low
Cyclohexane	280.49	268.85	26.33	0	Low
Toluene	318.6	299.85	29.77	0	0
R123	183.68	150.35	18.48	0.02	93

As for the NH_3–H_2O mixture, it is a reliable and proven fluid that makes it possible to produce a cooling effect at the temperatures required for refrigeration applications.

About the characteristics that make this system different from others found in the literature, we can count on the following:

- A deeper analysis of the dynamic behavior of the solar collector for a particular location, including the sizing of the thermal storage.
- A higher capacity for cooling over power production when compared to the Goswami systems, which prioritize power over cooling.
- A benefit of the power production as a result of the lower activation temperatures for the single-effect absorption cycle, regarding those required for double or triple-effect absorption cycles.
- A higher versatility of the proposed system to produce cooling suitable for refrigeration or air-conditioning applications due to the use of NH_3–H_2O Instead of H_2O–LiBr as other studies in the literature.

- A wider range of operating conditions is due to the higher heat source temperatures provided by the PTSC in comparison to other solar technologies proposed in similar studies.

Moreover, the analysis and presentation of the results in this work make it possible to assess the operation of the integrated configuration (ORC–ACS) with heat sources different than solar, such as industrial waste heat or geothermal energy, significantly expanding its potential applications and uses.

2. System Description

The thermal energy is supplied by the solar system (composed of the parabolic trough solar collector plus the storage system) to the integrated system (composed of the ORC and the ACS) through the heat transfer fluid (HTF), which, in this case, is pressurized water. The thermal energy absorbed ($\dot{q}$) by the HTF from the solar irradiation can be calculated using Equation (1) [69]:

$$\dot{q} = I_b A\, \eta_{opt}(\theta) Cos\theta - \dot{q}_{loss} \quad (1)$$

That thermal energy depends on the direct normal irradiation I_b, the aperture area A, the optical efficiency η_{opt}, the irradiation incidence angle adjustment factor $Cos\theta$, and the total thermal loss $\dot{q}_{loss}$.

The proposed ORC–ACS is presented in the schematic diagram in Figure 1, where the topping and bottoming cycles represent the ORC and ACS, respectively. In the ORC, the solar heat from the PTSC is supplied to the evaporator, increasing the temperature of the high-pressure stream coming from the pump and, thus, obtaining a superheated vapor at the exit of this component. The organic fluid in this state flows to the turbine, which is expanded to a lower pressure level, producing mechanical power that can be transformed into electricity by an electric generator. At the exit of the turbine, the organic fluid, remaining as a superheated vapor, enters into a closed-type heat exchanger where the power and cooling cycles are coupled. The fluid is condensed by rejecting its condensation heat to the concentrated solution in the generator of the absorption cycle. The organic fluid leaves this heat exchanger as saturated liquid and is pumped to the evaporator, thus closing the power cycle.

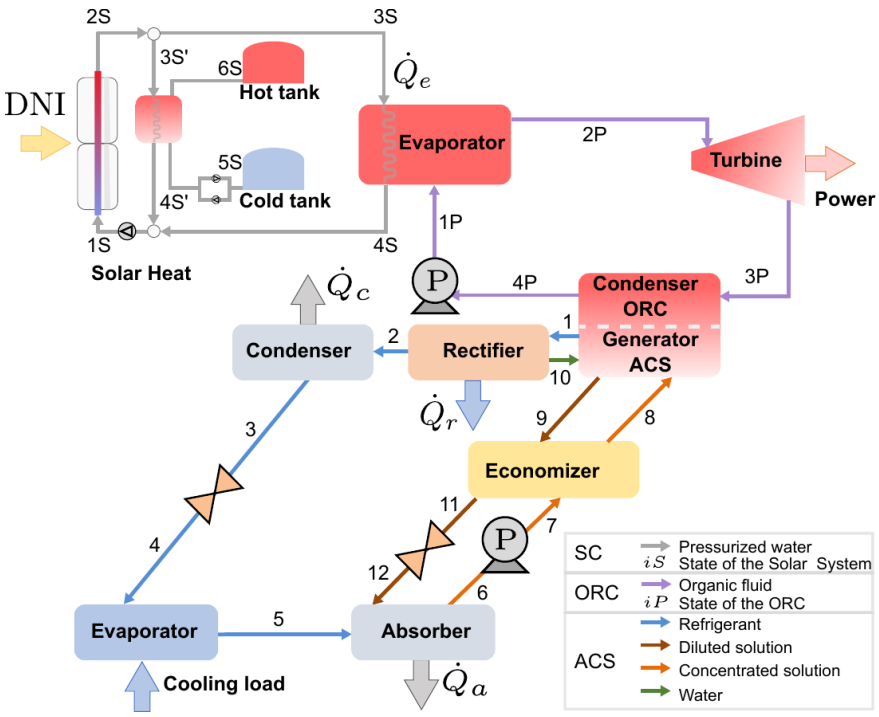

Figure 1. Schematic diagram of the integrated cooling and power system.

The condensation heat, transferred to the NH_3–H_2O solution in the ACS generator, produces a vapor-phase mixture of ammonia and steam (with a high ammonia concentration) and a liquid-phase NH_3–H_2O solution (with a low ammonia concentration). The vapor phase mixture flows through the rectifier, where part of the water is condensed and returned to the generator, thus maximizing the ammonia concentration of the vapor phase, which is liquefied in the condenser of the ACS by rejecting its condensation heat to an auxiliary cooling fluid. The condensed fluid is then expanded in a throttle valve to get the lowest pressure and temperature of the system.

The almost-pure ammonia at this condition has great potential to produce a cooling effect as it flows through the evaporator of the ACS. This component supplies an external thermal load to the working fluid, producing the desired cooling effect. The proposed model considers that, in this component, the working fluid is evaporated. Thus, the vapor-phase working fluid goes to the absorber, which is mixed with the liquid-phase NH_3–H_2O solution from the generator. The mixing process releases heat, which is recovered using an auxiliary cooling fluid. As a result of this process, an NH_3–H_2O solution with a high ammonia concentration is obtained and pumped back to the generator, closing the cycle. A heat exchanger identified as an economizer is included in the system to recover heat from the high-temperature solution flowing from the generator to the absorber and to transfer it to the solution stream flowing to the generator; thus, the economizer acts as an energy saver unit improving the system performance.

3. Mathematical Model

The model solution considered the following assumptions:

- The system operates in steady-state conditions.
- The system operates in thermodynamic equilibrium.
- There are no heat losses in components and piping.
- There are no pressure losses in components and piping.
- The process in the valve is isenthalpic.
- The condenser and absorber of the ACS operate at the same temperature.
- There is a constant temperature difference of 10 °C between the temperature of state 3P and states 1 and 9 in the generator of the ACS.

Some additional restrictions and definitions applicable to the model are presented in Table 2:

Table 2. Operative restrictions and definitions for the thermodynamic model of the cycle.

Consideration	Equation	Equation No.
Isentropic efficiency of pumps:	$\eta_P = 0.85$	(2)
Turbine isentropic efficiency:	$\eta_T = 0.85$	(3)
Effectiveness of the economizer:	$\varepsilon = \frac{h_8 - h_7}{h_9 - h_7} = 0.8$	(4)
Temperature at the output of the power cycle condenser	$80 \leq T_{4P} \leq 110$	(5)
Generation heat (known from the power cycle):	$\dot{Q}_g = \dot{m}_{1P}(h_{3P} - h_{4P})$	(6)
Generation temperature:	$T_9 = T_1 = T_{3P} - 10$	(7)
Condensing temperature:	$20 \leq T_3 = T_6 \leq 30$	(8)
Evaporation temperature:	$-10 \leq T_5 = T_{13} \leq 0$	(9)
Ammonia concentration after rectifier:	$y_2 = 0.999$	(10)
Ammonia concentration after evaporator:	$y_5 = 0.999$	(11)

The mass, ammonia, and energy balances in the main components of the integrated system are presented in Tables 3 and 4.

Table 3. Mass and ammonia balances for the main components of the ORC–ACS.

Component	Mass Balance	Equation No.	Ammonia Balance	Equation No.
ORC	$\dot{m}_{1P} = \dot{m}_{2P} = \dot{m}_{3P} = \dot{m}_{4P}$	(12)	/	/
Generator	$\dot{m}_6 = \dot{m}_1 + \dot{m}_9 - \dot{m}_{10}$	(13)	$\dot{m}_6 x_6 = \dot{m}_1 y_1 + \dot{m}_9 x_9 - \dot{m}_{10} x_{10}$	(14)
Rectifier	$\dot{m}_1 = \dot{m}_2 + \dot{m}_{10}$	(15)	$\dot{m}_1 y_1 = \dot{m}_2 y_2 + \dot{m}_{10} x_{10}$	(16)
Condenser	$\dot{m}_2 = \dot{m}_3$	(17)	$\dot{m}_2 y_2 = \dot{m}_3 x_3$	(18)
Valve 1	$\dot{m}_3 = \dot{m}_4$	(19)	$\dot{m}_3 x_3 = \dot{m}_4 x_4$	(20)
Evaporator	$\dot{m}_4 = \dot{m}_5$	(21)	$\dot{m}_4 x_4 = \dot{m}_5 y_5$	(22)
Absorber	$\dot{m}_9 + \dot{m}_5 = \dot{m}_6$	(23)	$\dot{m}_9 x_9 + \dot{m}_5 y_5 = \dot{m}_6 x_6$	(24)
Pump	$\dot{m}_6 = \dot{m}_7$	(25)	$\dot{m}_6 x_6 = \dot{m}_7 x_7$	(26)
Valve 2	$\dot{m}_{11} = \dot{m}_{12}$	(27)	$\dot{m}_{11} x_{11} = \dot{m}_{12} x_{12}$	(28)

Table 4. Energy balances for the main components of the ORC–ACS.

Component	Energy Balance	Equation No.
Generator	$\dot{Q}_g = \dot{m}_1 h_1 + \dot{m}_9 h_9 - \dot{m}_{10} h_{10} - \dot{m}_6 h_6$	(29)
Rectifier	$\dot{Q}_r = \dot{m}_1 h_1 - \dot{m}_2 h_2 - \dot{m}_{10} h_{10}$	(30)
Condenser ACS	$\dot{Q}_c = \dot{m}_2 (h_2 - h_3)$	(31)
Valve 1	$\dot{m}_3 h_3 = \dot{m}_4 h_4$	(32)
Evaporator ACS	$\dot{Q}_e = \dot{m}_5 h_5 - \dot{m}_4 h_4$	(33)
Absorber	$\dot{Q}_a = \dot{m}_9 h_9 + \dot{m}_5 h_5 - \dot{m}_6 h_6$	(34)
Pump ACS	$\dot{W}_{P,ACS} = v_6 (P_7 - P_6)$	(35)
Valve 2	$\dot{m}_{11} h_{11} = \dot{m}_{12} h_{12}$	(36)
Evaporator ORC	$\dot{Q}_{e,ORC} = \dot{m}_{1P} (h_{2P} - h_{1P})$	(37)
Turbine	$\dot{W}_T = \dot{m}_{1P} (h_{2P} - h_{3P})$	(38)
Condenser ORC	$\dot{Q}_{c,ORC} = \dot{m}_{1P} (h_{3P} - h_{4P})$	(39)
Pump ORC	$\dot{W}_{P,ORC} = v_6 (P_{1P} - P_{4P})$	(40)

The performance parameters for the integrated system are the Energy Utilization Factor (EUF) and the Exergy Efficiency (η_{II}), which are defined as indicated by Equations (41) and (42), respectively.

$$EUF = \frac{\left(\dot{Q}_E + \dot{W}_{T,ORC,a}\right)}{\dot{Q}_{E\ ORC} + \dot{W}_{P,ORC,a} + \dot{m}_6 w_{P,a}} \tag{41}$$

$$\eta_{II} = \frac{\dot{Q}_E \left(1 - \frac{T_5 + 10}{298.15}\right) + \dot{W}_T}{\dot{Q}_{E,ORC} \left(1 - \frac{298.15}{T_{2P} + 10}\right) + \dot{W}_P + \dot{W}_{P,ORC}} \tag{42}$$

In Equation (42), temperatures are expressed in the thermodynamic scale, and a difference of 10 °C is added to the lowest and highest temperatures of the integrated cycle to consider that cooling and heating are related to external heat sources. In this equation, the numerator represents the exergy of the cooling load and power produced, while the denominator is the sum of the exergy of the work and heat supplied to the integrated system in the pumps and in the ORC evaporator.

Model Validation

The model validation was conducted considering the integrated system as the coupling of three independent systems: the solar, power, and cooling systems. The independent systems validation is presented next.

The solar system was modeled using the NREL's System Advisor Model (SAM 2022.11.21) software, which is an open-source project that allows the design of techno-economic models of renewable energy, including the parabolic trough technology chosen for this study; this particular model had been previously validated with experimental data [69].

On the other hand, the results of the power model were compared to those reported by Mohammadi et al. [70], while the corresponding absorption model was contrasted to those reported by Clerk and Trezek [71]. Both references were chosen since the analyzed cycles are similar to those in the present configuration. Moreover, both references were adequately validated. The main validation findings for a specified operating condition are presented in Table 5.

Table 5. Comparison of the main results obtained with this model and data in the literature [70].

System	Parameter	Present Work	Mohammadi et al. [70]	Units	Relative Error (%)
ORC	Turbine power	7.42	7.317	kW	1.41
	Pump power	0.1519	0.156	kW	2.63
	Efficiency	34.19	32.27	%	5.95
System	Parameter	Present work	Clerk and Trezek [71]	Units	Relative error (%)
Absorption cycle	Cooling load	10.5	10.51	kW	0.10
	Generation load	21.78	21.66	kW	0.55
	X_{conc}	0.44	0.41	--	7.32
	X_{dil}	0.29	0.28	--	3.57
	COP	0.48	0.47	--	2.13

From the validation analysis, it is observed that, for the power cycle, a good agreement is achieved for the power of the turbine and pump, as well as for the efficiency of the cycle.

As for the absorption cycle, it was found that the main differences were obtained for the concentration of the strong and weak solutions, with the maximum approximated to 7%; however, in general, a good agreement was observed for the proposed model regarding the chosen references in the literature.

4. Results

As a reference for the readers, Table 6 outlines the main operational parameters of the integrated system as well as the thermal loads and performance parameters during its instantaneous operation on 21 June at 12:00, coinciding with the summer solstice at noon. This specific date and time have been chosen as a representative point for comparison purposes. Additionally, the data in Table 6 are presented with Benzene as the Organic Rankine Cycle (ORC) working fluid. This selection is based on subsequent results presented in this section, where Benzene emerged as the optimal fluid among those analyzed in terms of performance.

Table 6. Operative parameters for the integrated system on June 21 at 12 h.

State (See Figure 1)	Mass Flow Rate (kg/s)	T (°C)	P (kPa)	Composition (%)	Specific Enthalpy (kJ/kg)
		Solar system			
1S	1	168.1	2300	100	711.84
2S	1	197.1	2300	100	839.79
3S	0.6135	197.1	2300	100	839.79
3S′	0.3864	197.1	2300	100	839.79
4S	0.6135	170	2300	100	720.13
4S′	0.3864	170	2300	100	720.13
		Organic Rankine Cycle			
1P	0.1415	100.5	1162	100	40.17
2P	0.1415	187.1	1162	100	524.6
3P	0.1415	129.4	180.2	100	459.7
4P	0.1415	100	180.2	100	38.71
		Absorption Cooling Cycle			
1	0.03486	119.4	857.2	0.8081	1752
2	0.026	109.4	857.2	0.9996	1516
3	0.026	20	857.2	0.9996	93.37
4	0.026	−26.8	139.3	0.9996	93.37
5	0.026	−5	139.3	0.9996	1284
6	0.1069	20	139.3	0.3981	−138.3
7	0.1069	20	857.2	0.3981	−137.4
8	0.1069	86.2	857.2	0.3981	272.8
9	0.08091	119.4	857.2	0.2049	375.3
10	0.008866	109.4	857.2	0.2465	310.3
11	0.08091	−6.7	857.2	0.2049	−166.6
12	0.08091	−6.5	139.3	0.2049	−166.6
		Power			
System	Location		Thermal load		Units
Solar energy	DNI		168.26		kW_{th}
Solar system	PTSC		127.94		kW_{th}
Solar system	$\dot{Q}_e$		73.41		kW_{th}
ORC	$\dot{Q}_e$		68.51		kW_{th}
ORC	$\dot{Q}_c$		59.55		kW_{th}
ORC	$\dot{W}_T$		9.17		kW
ACS	$\dot{Q}_g$		59.55		kW_{th}
ACS	$\dot{Q}_c$		36.98		kW_{th}
ACS	$\dot{Q}_a$		34.69		kW_{th}
ACS	$\dot{Q}_e$		30.96		kW_{th}
		Performance			
Parameter			Value		Units
η_{ORC}			13.08		%
COP			51.9		%
EUF			58.31		%
η_{Ex}			44.3		%

4.1. Solar System

As previously mentioned, the design of the thermal supply to the cooling and power system is based on a parabolic trough model. The solar system is composed of the parabolic trough collector and the storage system; its performance was calculated using the SAM (2022.11.21 version) software, which allows the estimation of techno-economic aspects of renewable energy projects. The main parameters required to carry out the solar system simulation are site location, design point, solar multiple, heat transfer fluid (HTF), thermal storage, design thermal power, and type of parabolic collector. Site selection requires

knowledge of the available solar resources; for solar concentration, it is recommended that the site have a direct daily irradiance above 5 kWh/m^2 [72]. The site selected for this project is located in the city of Temixco, Morelos, Mexico, at coordinates 18.8393° N and −99.2354° E. This location experiences a daily irradiance of 6.58 kWh/m^2, a value higher than the recommended threshold. The design point parameter is determined by calculating the cumulative distribution of the direct normal irradiance (DNI) of a typical meteorological year (TMY) and selecting the value that represents the 95th percentile of the distribution. For the selected site, this value is 950 W/m^2. Figure 2 displays the daily solar energy availability per square meter at the selected site for each month, along with an hourly map illustrating irradiance throughout the year.

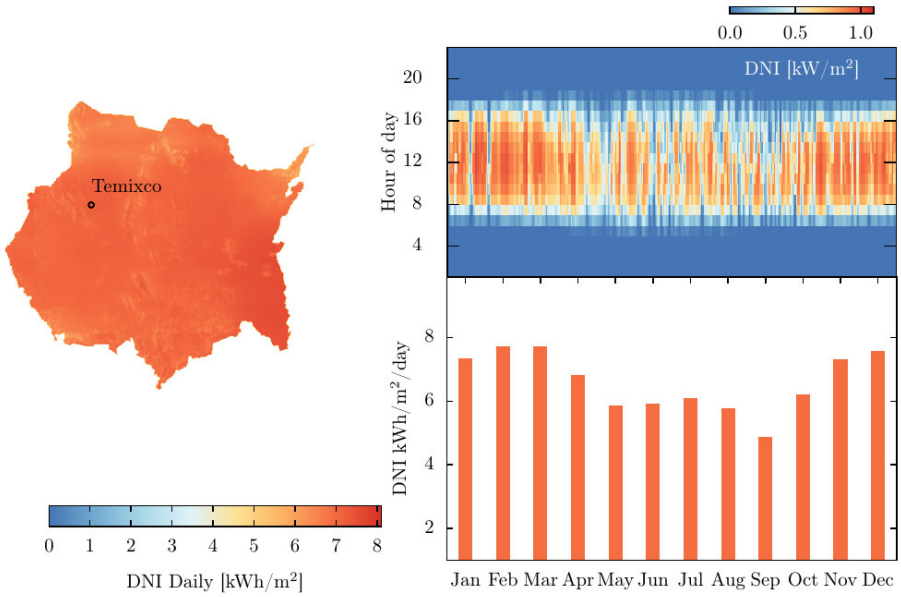

Figure 2. Average insolation and irradiance for the analyzed site.

The solar multiple (SM) is the ratio between the thermal power of the receiver and the thermal power delivered by the solar system. This value is utilized to dimension the receiver's power. When SM = 1, the solar irradiance incident on the receiver generates the design thermal power for only a few hours throughout the year. On the other hand, if SM > 1, there will be more hours throughout the year in which the design demand is satisfied. Accomplishing the design demand for a longer time usually includes a storage system that allows the supply of thermal energy in adequate conditions for a longer period. The SM used in this model is 1.5.

The choice of the HTF depends on the required temperatures. The SAM software allows the selection of various types of HTF, including oils, molten salts, or pressurized water. Considering that the operating temperature range is not extreme, pressurized water is preferred for this model. The temperature range in the model is as follows: the supposed HTF temperature entering the collector is 170 °C, while the expected outlet temperature is 210 °C. According to the simulation results, Figure 3 presents the HTF temperature achieved by the PTSC by hour throughout the year.

In Figure 3, it is possible to identify the three main periods: a main period, from 8 to 16 h, when the PTSC is the main heat provider to the integrated system but also to the storage system; a secondary period, from 16 to 24 h, when the thermal energy to the integrated system is provided mainly by the storage system; and a third period, from 24 to 8 h, when the HTF temperature is the lowest due to the intermittent behavior of solar energy and the specified capacity of the thermal storage.

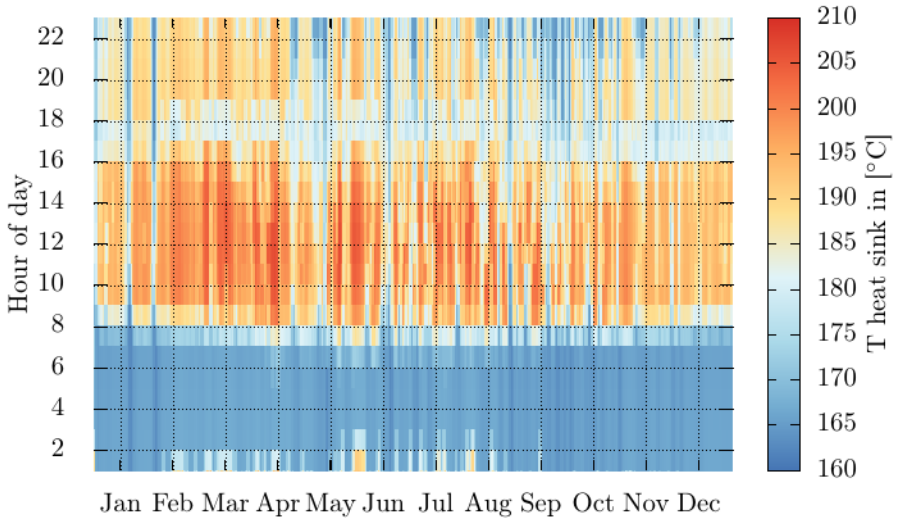

Figure 3. Solar system outlet temperature.

It was found that, for the chosen site, considering a continuous operation (24/7), a mean HTF temperature delivered by the solar system (T_s) of 180.8 °C (±12.9 °C) can be achieved with the solar system. However, if it is considered the operation of the integrated system only in the main period, the mean HTF temperature can reach up to 192.7 °C (±9.1 °C). This value diminishes to 187.5 °C (±10.2 °C) considering the main and secondary periods when the PTSC and the storage system supply the heat.

On the other hand, it is possible to indicate the desired thermal power to be delivered by the solar system ($\dot{Q}_s$); however, based on the chosen operative conditions, the software will determine if the system can achieve that power. In this case, the thermal power desired was 100 kW. Figure 4 shows the predicted thermal power that the solar system can deliver throughout the year; as in the case of the HTF temperatures, the characteristics of the thermal power can also be described based on the period chosen for the analysis. A mean thermal power up to 58 kW (±22.1 kW) can be reached in the main period, but that value is just 45.2 kW (±24.2 kW) when main and secondary periods are considered (8 to 24 h) and hardily 30 kW (±28.5 kW) when a continuous operation (24/7) is considered.

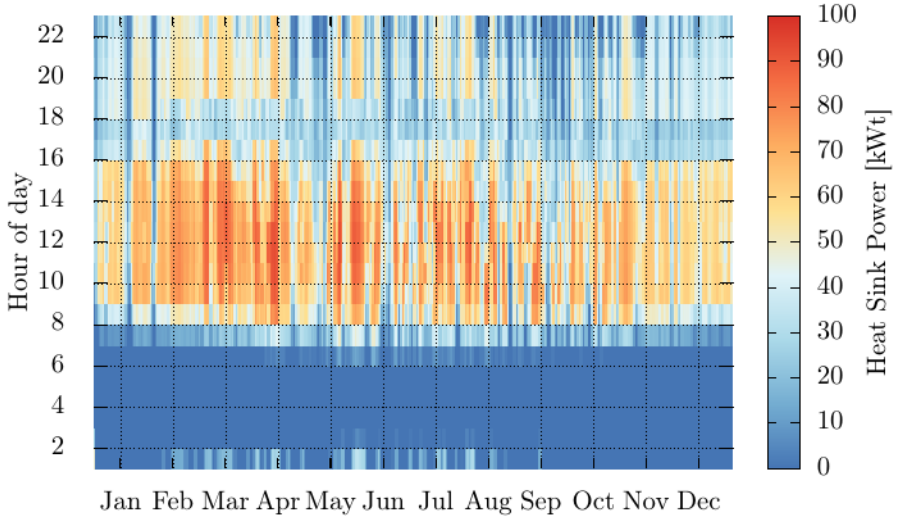

Figure 4. Solar system thermal power.

The previous results correspond to the parabolic trough model *Luz LS-2*, which is the smallest collector from those available for selection in the software utilized for the modeling. It has a reflective aperture area of 235 m^2 (width = 5 m, length = 49 m) with a receiver with an internal diameter of the absorber tube of 76 mm. The thermal power achieved by the current solar configuration (parabolic trough + storage system) is significantly lower than the thermal power considered at the design point (100 kW). It means that whether a project demands to supply a heating load of 100 kW, either a bigger collector model should be chosen, or more than one collector would be required to accomplish the thermal requirement. The analysis of the integrated system in the next section will consider the current configuration of the solar system.

Regarding thermal storage, a storage period of 10 h was considered the design point. Two tanks with an HTF volume of 25 m^3 were considered for storage. The analysis did not include any external heater for the storage tanks. A heat loss in the storage system of 10 kW is estimated. The thermal behavior of this system is shown in Figure 5, which characterizes the charge and discharge cycles and the HTF temperature variation. These parameters correspond to 7 and 8 January. Figure 5 demonstrates that the charging process of the storage system starts at 8 h from the first moment of solar energy availability. It is also shown that, in appropriate conditions, the system can quickly reach its maximum storing capacity (50 kW). On the other hand, the discharge process starts once the collection of solar energy ceases; it is on 7 January, at 18 h. At this date, the storage system can provide thermal energy for approximately 6 h (second analysis period). As for the HTF temperatures in the storage system, a maximum value near 190 °C is achieved at 17 h, which means that contrary to the thermal power, it keeps increasing as the sunlight is available. The minimum temperature in the storage system is near 150 °C, reached just before the charging process starts.

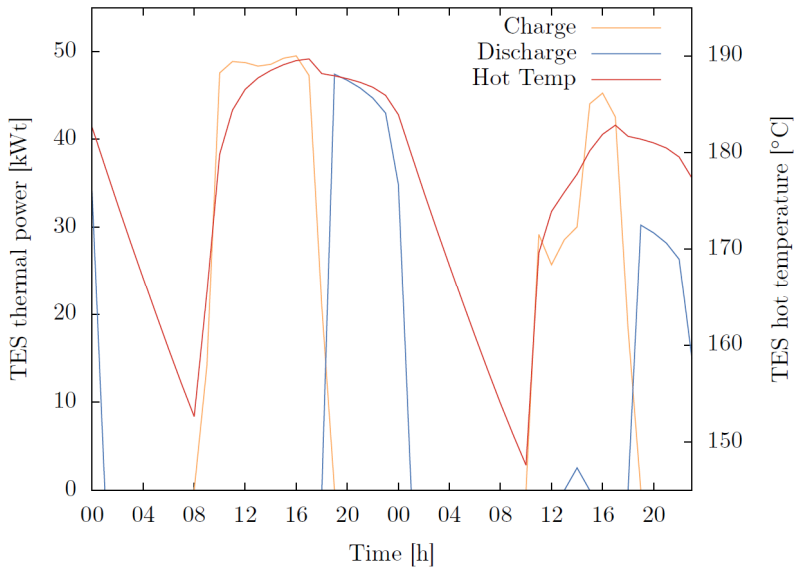

Figure 5. Storage system thermal performance.

4.2. Integrated Cooling and Power System

The performance analysis of the integrated system for cooling and power is conducted using the results of the solar system operation during the main and secondary periods, that is, considering the average thermal power and HTF temperature supplied by the solar system from 8 to 24 h. Both parameters T_s = 187.5 °C(±10.2 °C), and $\dot{Q}_s$ = 45.2 kW (±24.2 kW), are kept constant for the analysis of the integrated ORC–ACS.

As for the integrated cooling and power system (ORC–ACS), the main input parameters are the temperatures of the thermodynamic states designed as 4P (ORC), 3 (ACS), and 5 (ACS). T_{4P} defines the low pressure of the ORC, thus limiting the expansion of the

organic fluid in the turbine and affecting the temperature of the heat transferred to the NH_3–H_2O in the generator of the ACS. This parameter is varied as 80 °C $\leq T_{4P} \leq$ 110 °C. T_3 is defined by the cooling fluid in the condenser and absorber ($T_3 = T_6$). The model considers temperatures T_3 and T_6 10 °C higher than the cooling fluid temperature. The cooling fluid in the condenser and absorber is commonly water or even air at ambient temperature, which is a time-dependent variable. Thus, this model considers T_3 to vary in the range 20 °C $\leq T_3 = T_6 \leq$ 30 °C. Finally, the T_5 represents the cooling temperature achieved by the ACS. This value depends on the application of the cooling system, and for the modeling purpose, T_5 will be varied between −10 °C and 0 °C.

Since the heat power and the HTF temperature supplied to the ORC by the solar system are fixed, the only variables affecting the ORC performance are T_{4P} and the organic fluid. The ORC performance as a function of both parameters is shown in Figure 6, where it is shown that benzene is the best fluid to get the highest turbine power and thermal efficiency for the ORC. It is evident from Figure 6 that ORC power and efficiency decrease as the organic fluid temperature leaving the condenser increases. It is an expected behavior because this temperature is proportional to the low pressure in the system; thus, an increment in that temperature augments the discharge pressure of the turbine, reducing the expansion process and the ORC efficiency.

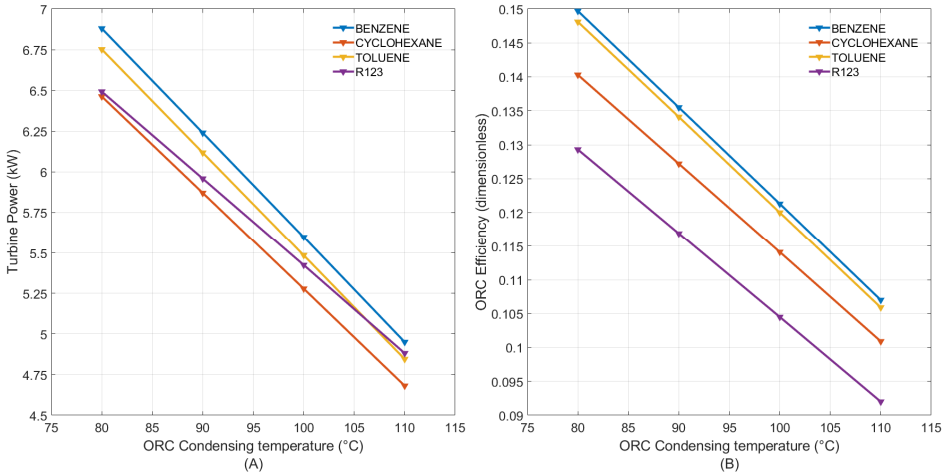

Figure 6. Organic fluid and condensing temperature effects on the (**A**) turbine power, and (**B**) ORC efficiency.

Once the organic fluid effect on the power cycle has been analyzed, the following results will consider the use of benzene in the ORC. Figure 7 analyzes the ACS performance as a function of the condensing and cooling temperatures; such results are determined for $T_{4P} = 100$ °C.

Figure 7 presents the effect of condensing (T_3) and cooling (T_5) temperatures on the cooling load and the performance of the ACS. As was hoped, increasing the condensing temperature significantly affects the performance of the absorption system. The cooling temperature follows the same trend: decreasing this parameter while keeping constant the heat source temperature represents a more significant challenge for the cooling system; it is observed as a detriment to the cooling power and, thus, on the COP. Since the cooling temperature of −10 °C effect on the ACS performance is more evident than that for the other cooling temperatures, the following results, describing the performance of the integrated system were obtained considering $T_5 = -5$ °C.

The simultaneous variation of the main parameters for the integrated system, the cooling load and the turbine power, can be analyzed as a rate for different ORC and ACS condensing temperatures, as shown in Figure 8, where it is evident that the higher ORC condensing temperature, the more cooling load obtained.

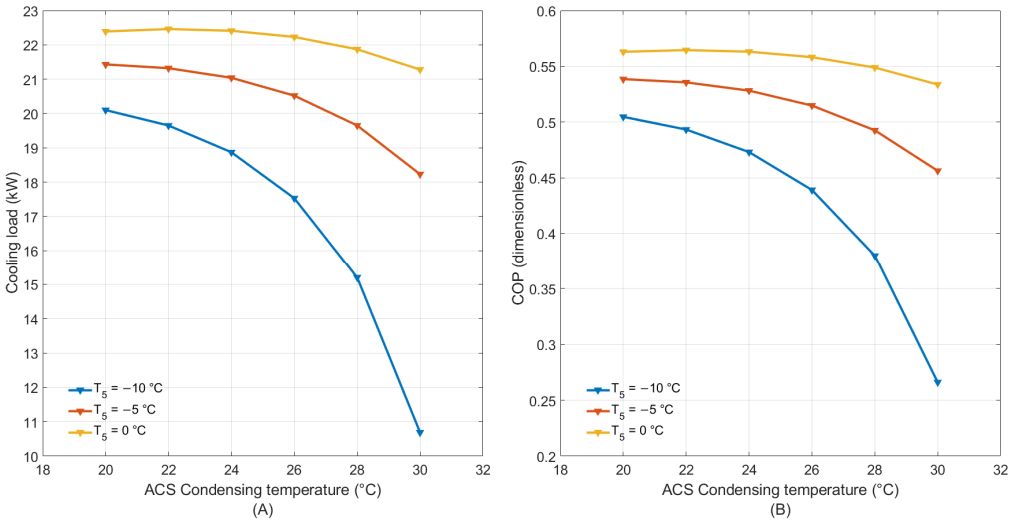

Figure 7. ACS condensing temperatures effect on (**A**) cooling load and (**B**) COP.

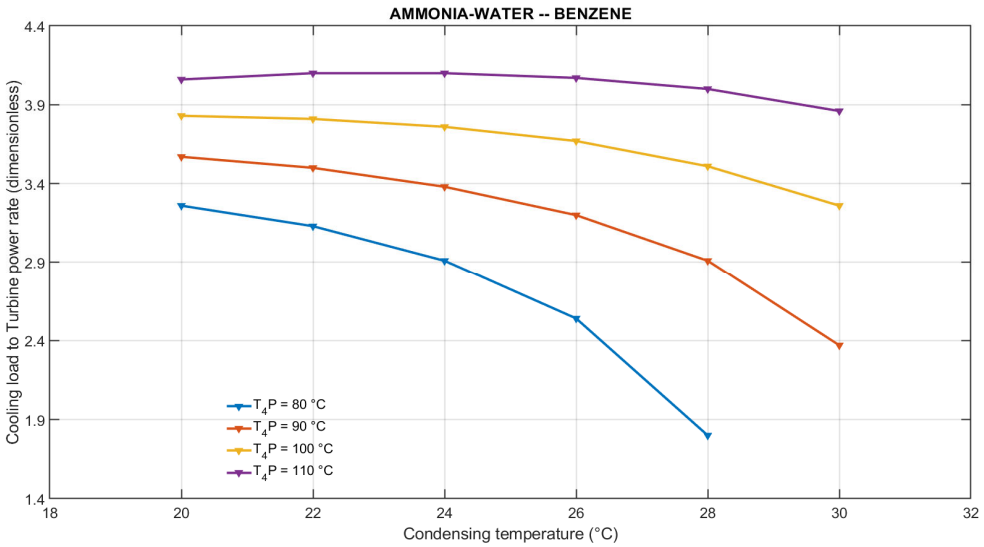

Figure 8. Condensing and cooling temperatures' effect on the cooling load to turbine power rate.

Figure 9A presents EUF as a function of the ORC and ACS condensing temperature at a −5 °C cooling temperature using benzene as the organic fluid in the ORC. As previously analyzed, the ACS condensing temperature affects the cooling power and then the EUF; however, this figure shows that EUF is also highly dependent on the ORC condensing temperature. Figure 9A shows that although for low ORC condensing temperatures, the condensation in the ACS at low temperatures favors the EUF and the organic fluid expansion (and thus the power production), the performance at this condition is affected to a greater extent when the ACS condensing temperature increases. Thus, since the ACS condensing temperature is a variable depending on time, it is recommended to operate the integrated system at ORC condensing temperatures above 100 °C. At such conditions, more stability in the system performance would be obtained.

On the other hand, Figure 9B shows that, although for a 110 °C ORC condensing temperature, the organic fluid with the highest performance is R123 (at low ACS condensing temperatures), the system performance using this fluid is the most dependent on the ACS condensing temperatures. Thus, the utilization of R123 in the proposed system is not recommended. For the remaining organic fluids, Figure 9B corroborates that benzene is the best option from the analyzed fluids since, for any ACS condensing temperature, the best system performance is achieved with this fluid.

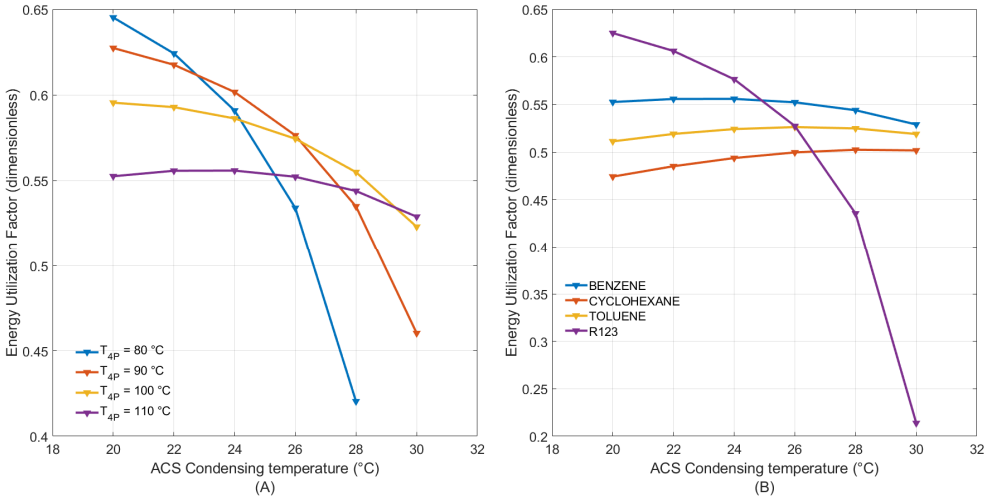

Figure 9. (**A**) EUF as a function of ORC and ACS condensing temperatures for benzene; (**B**) EUF as a function of organic fluids and ACS condensing temperatures at T_{4P} = 110 °C.

The system exergy efficiency is presented in Figure 10A, which shows that, as for the EUF, the second-law efficiency is affected by an increment of the ACS condensing temperature, as the performance at low ORC condensing temperatures is more affected by that parameter. It was found that the theoretical performance for the integrated system is not possible for ORC and ACS condensing temperatures of 80 °C and 30 °C, respectively. It means that 80 °C is near the lowest operating condition to condense the organic fluid for a cooling fluid temperature above 25 °C, which is usually taken as a standard environment temperature in theoretical studies.

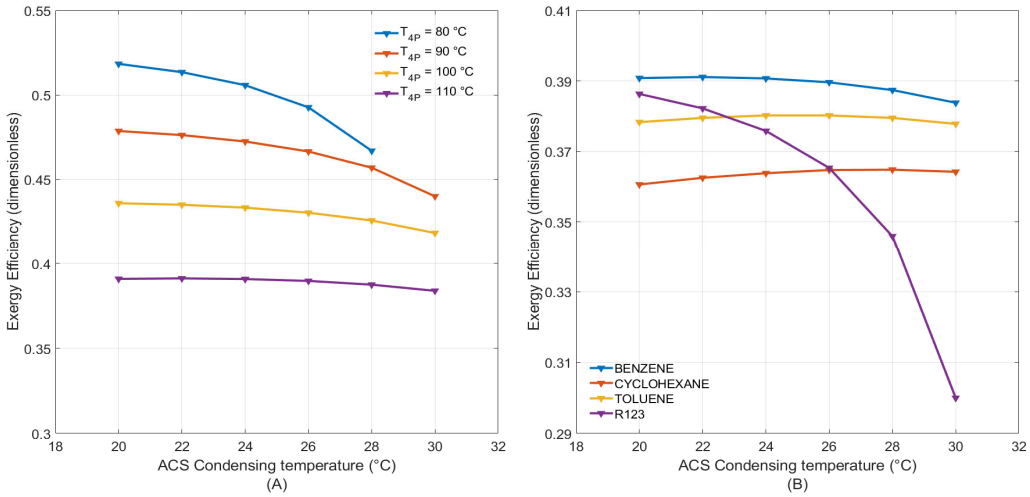

Figure 10. (**A**) Exergy efficiency as a function of ORC and ACS condensing temperatures for benzene; (**B**) exergy efficiency as a function of organic fluids and ACS condensing temperatures at T_{4P} = 110 °C.

Figure 10B shows the exergy performance for the analyzed organic fluids when they are condensed at 110 °C. It is proved that R123 remains the least recommended fluid to be used in the ORC; although the organic fluid is only present in the topping cycle, it affects the heat source temperature of the bottoming cycle, causing its poor performance at high condensing temperatures, as Figure 10B shows. At difference from the EUF presented in Figure 9B, for an ORC condensing temperature of 110 °C, the best exergy efficiency is obtained with benzene, regardless of the ACS condensing temperature.

From Figures 9 and 10, it is evident that when R123 is used in the power cycle, the performance of the integrated system is highly affected by the condensing temperature of the absorption system. Although it seems contradictory, it is because when using R123 on

the power system, the heat load from the upper to the bottoming cycle is transferred at a lower temperature in comparison to the other organic fluids analyzed (for the condition presented, 20 °C lower than in the case of benzene); operating the system in limit conditions regarding the heat source temperature, hence, if in addition, the condensation temperature increases, it results in detriment of the system performance, as shown by the EUF and the exergy efficiency.

Figure 11 shows the hourly performance of the integrated system according to the first (COP, ORC efficiency, and EUF) and second (Exergy efficiency) laws; for the spring equinox (Figure 11A), summer solstice (Figure 11B), autumn equinox (Figure 11C), and winter solstice (Figure 11D), considering a cooling temperature of −5 °C and a condensing temperature for the organic fluid (T_{4P}) of 100 °C.

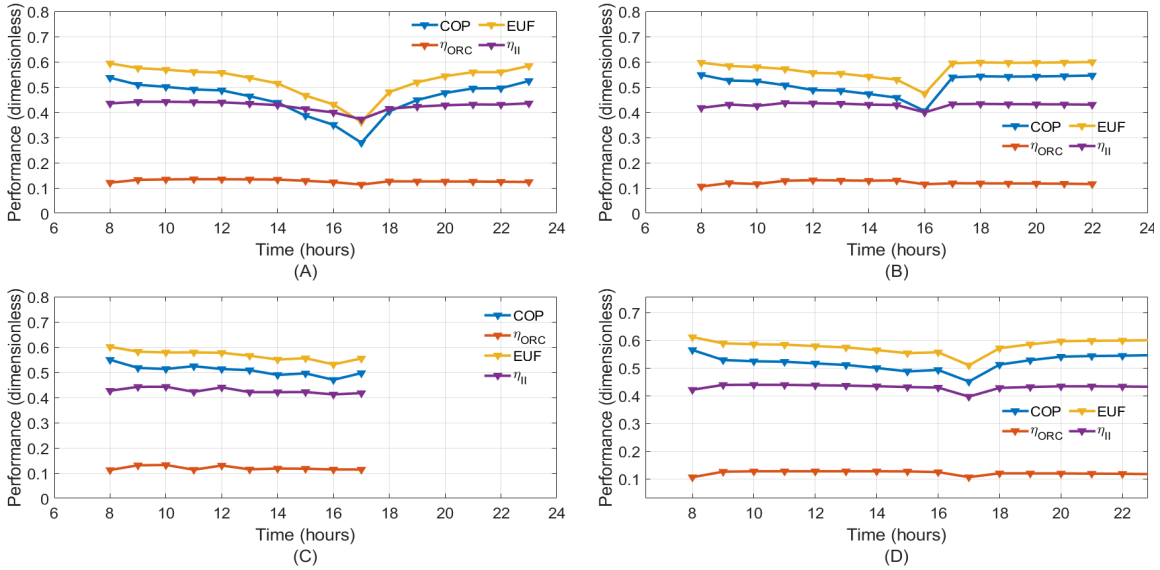

Figure 11. Predicted hourly performance of the integrated system for the spring equinox (**A**), summer solstice (**B**), autumn equinox (**C**), and winter solstice (**D**).

It is evident from Figure 11 the time when solar energy is no longer available, and the storage system starts providing the thermal energy to drive the integrated system (around 16 or 17 h), except for the autumn equinox (21 September) when the storage system is not able to supply energy to the cooling and power system due to the rainy season in the chosen location. The low availability of solar energy for this season can be seen in Figure 2.

It is also shown that, in general, the proposed storage system supplies thermal energy, maintaining the performance achieved with the PTSC, and even, in some cases, reaching higher and more steady values for parameters like EUF and COP. This is because the storage system supplies energy at similar or even slightly higher temperatures than the PTSC does at the end of the solar day (first period of analysis); thus, parameters such as the exergy efficiency are not significantly affected by the heat source (PTSC or storage system).

Comparing the results obtained of the proposed system with others for the same purposes utilizing ORCs and ACSs, it was observed that the EUF (0.42–0.65) were lower with the proposed system than those obtained by Jiménez et al. [58] (0.62–0.76), but the exergy efficiencies were considerably higher (0.39–0.52) than those reported in that work (0.14–0.36). This is because Jimenez et al. [58] analyzed a double-stage ACS, which is more efficient than the single-effect system used in the present study; however, that system requires higher driving temperatures, increasing the system irreversibilities. Comparing the results with those obtained by Pashapour et al. [57], the exergy values are similar since they reported a maximum exergy efficiency of 0.50. Finally, comparing the results with those obtained in the study realized by Sharifishourabi and Chadegani [55], the results were better since they obtained 0.39, 1.34, and 14.4% for EUF, COP, and exergy efficiency,

respectively, while in the present study, higher values were obtained except the COP since they utilized a triple-effect cooling system which is more efficient than the single-effect system modeled in the present study.

5. Conclusions

The present study proposed and analyzed the performance of an integrated power and cooling system operated with solar energy in Temixco, Morelos, Mexico. The proposed solar energy collection system consisted of a commercial parabolic trough solar collector (PTSC) and a thermal energy storage (TES) system. The potential for harnessing solar energy was evaluated using the SAM (2022.11.21 version) software from NREL. The thermal power and temperature available at the interest site were presented considering three periods per day, of 8 h each. Based on this information, it was determined that the proposed solar system could supply power close to 45 kW at a temperature of approximately 187.5 °C, annual average, for the period between 8 and 24 h. With these results, the integrated system was evaluated for simultaneous power and cooling production, finding that, among the organic fluids analyzed, benzene offers the greatest theoretical potential for improving the integrated system's first and second law performance. Furthermore, it was found that using R123 as a working fluid for the power cycle is not convenient for the performance of the integrated system due to the relatively low heat supply temperatures to the absorption system for most of the operating conditions analyzed. The maximum value for the EUF was 0.6841, which was obtained with benzene as the ORC working fluid at the ORC and ACS condensation temperatures of 80 °C and 20 °C, respectively, and at a cooling temperature of 0 °C; these conditions favor the expansion of the organic fluid and the operation of the absorption system. However, the best exergy performance (0.5239) was obtained when the cooling temperature was −10 °C instead of 0 °C because this condition represents a greater temperature difference for the high- and low-temperature thermal sources of the cooling system, which favors its second-law performance.

As for the limitations of the present study, we consider that cascade configuration for the power and cooling cycles, as proposed in the present study, limits the power production since the condensation heat in the power cycle must be at a temperature high enough to activate the absorption system. This limitation could be surpassed if the heat source is high enough to allow higher pressures appropriate to the organic cycle at the turbine inlet. In this regard, a challenge to overcome relates to the maximization of power production by taking advantage of the heat source instead of reducing the cooling load by the proposal of new configuration modes, as could be that allowing the heat to be supplied to both cycles (power and cooling) and not only to the power cycle. This kind of theoretical study, as well as the setting up of an experimental facility coupling the power and cooling cycles at a small scale (in the first place), is considered the future research to be explored, in which the main challenge would be the design of a small-scale turbine appropriate to take advantage of the fluid and operating conditions reported in this study.

Finally, it is concluded that although the proposed system could be a technically feasible option for satisfying a simultaneous cooling and power demand, it is necessary to develop an economic study to determine its profitability.

Author Contributions: Conceptualization, W.R.; methodology, W.R.; software, J.C.J.-G. and I.M.-C.; validation, J.C.J.-G. and I.M.-C.; formal analysis, J.C.J.-G. and I.M.-C.; investigation, W.R.; resources, J.C.J.-G., I.M.-C. and W.R.; data curation, J.C.J.-G. and I.M.-C.; writing—original draft preparation, J.C.J.-G. and I.M.-C.; writing—review and editing, W.R.; visualization, J.C.J.-G. and I.M.-C.; supervision, W.R.; project administration, J.C.J.-G.; funding acquisition, J.C.J.-G. All authors have read and agreed to the published version of the manuscript.

Funding: This work was carried out with the support of the PAPIIT-DGAPA (UNAM) project number IA106423, titled "Evaluación experimental de sistemas de enfriamiento por absorción con mezclas de trabajo alternativas".

Data Availability Statement: The raw data supporting the conclusions of this article will be made available by the authors on request.

Acknowledgments: Isaías Moreno Cruz acknowledges the postdoctoral fellowship awarded by CONACYT through the program "Estancias Posdoctorales por México 2022(1)" agreement I1200/320/2022.

Conflicts of Interest: The authors declare no conflict of interest.

Nomenclature

ACS	Absorption Cooling Systems
COP	Coefficient of Performance
DNI	Direct Normal Irradiance
ERC	Ejector Refrigeration Cycles
EUF	Energy Utilization Factor
HTF	Heat Transfer Fluid
ORC	Organic Rankine Cycle
PTSC	Parabolic Trough Solar Collector
SAM	System Advisor Model
SM	Solar Multiple
TMY	Typical Meteorological Year
VCRC	Vapor Compression Refrigeration Cycles

Subscripts

A	Absorber
C	Condenser
conc	Relative to the NH_3-H_2O concentrated solution
dil	Relative to the NH_3-H_2O diluted solution
E	Evaporator
EC	Economizer
G	Generator
P	Pump

Symbols

$\dot{m}$	Mass flow rate
$\dot{Q}$	Thermal load
η	Efficiency
T	Temperature
x	Ammonia concentration in the liquid-phase
y	Ammonia concentration in the vapor-phase
$\dot{W}$	Power

References

1. BP. *Statistical Review of World Energy*; BP: London, UK, 2022.
2. Ahmed, S.F.; Khalid, M.; Vaka, M.; Walvekar, R.; Numan, A.; Rasheed, A.K.; Mubarak, N.M. Recent progress in solar water heaters and solar collectors: A comprehensive review. *Therm. Sci. Eng. Prog.* **2021**, *25*, 100981. [CrossRef]
3. Zhai, H.; An, Q.; Shi, L.; Lemort, V.; Quoilin, S. Categorization and analysis of heat sources for organic Rankine cycle systems. *Renew. Sustain. Energy Rev.* **2016**, *64*, 790–805. [CrossRef]
4. Zhang, X.; Zhang, C.; He, M.; Wang, J. Selection and Evaluation of Dry and Isentropic Organic Working Fluids Used in Organic Rankine Cycle Based on the Turning Point on Their Saturated Vapor Curves. *J. Therm. Sci.* **2019**, *28*, 643–658. [CrossRef]
5. Bianchi, M.; Branchini, L.; De Pascale, A.; Melino, F.; Ottaviano, S.; Peretto, A.; Torricelli, N. Performance and total warming impact assessment of pure fluids and mixtures replacing HFCs in micro-ORC energy systems. *Appl. Therm. Eng.* **2021**, *203*, 117888. [CrossRef]
6. Bahrami, M.; Pourfayaz, F.; Kasaeian, A. Low global warming potential (GWP) working fluids (WFs) for Organic Rankine Cycle (ORC) applications. *Energy Rep.* **2022**, *8*, 2976–2988. [CrossRef]
7. Blondel, Q.; Tauveron, N.; Lhermet, G.; Caney, N. Zeotropic mixtures study in plate heat exchangers and ORC systems. *Appl. Therm. Eng.* **2023**, *219*, 119418. [CrossRef]
8. Lu, J.; Zhang, J.; Chen, S.; Pu, Y. Analysis of organic Rankine cycles using zeotropic mixtures as working fluids under different restrictive conditions. *Energy Convers. Manag.* **2016**, *126*, 704–716. [CrossRef]

9. Geng, D.; Du, Y.; Yang, R. Performance analysis of an organic Rankine cycle for a reverse osmosis desalination system using zeotropic mixtures. *Desalination* **2016**, *381*, 38–46. [CrossRef]
10. Sadeghi, M.; Nemati, A.; Ghavimi, A.; Yari, M. Thermodynamic analysis and multi-objective optimization of various ORC (organic Rankine cycle) configurations using zeotropic mixtures. *Energy* **2016**, *109*, 791–802. [CrossRef]
11. Luo, X.; Huang, R.; Yang, Z.; Chen, J.; Chen, Y. Performance investigation of a novel zeotropic organic Rankine cycle coupling liquid separation condensation and multi-pressure evaporation. *Energy Convers. Manag.* **2018**, *161*, 112–127. [CrossRef]
12. Ahmed, A.M.; Imre, A.R. Investigation of thermal efficiency for subcritical ORC and TFC using super dry working fluids. *Energy Sci. Eng.* **2023**, *11*, 711–726. [CrossRef]
13. Zhang, X.; Li, Y. An examination of super dry working fluids used in regenerative organic Rankine cycles. *Energy* **2023**, *263*, 125931. [CrossRef]
14. Maali, R.; Khir, T. Thermodynamic analysis and optimization of an ORC hybrid geothermal–solar power plant. *Euro-Mediterranean J. Environ. Integr.* **2023**, *8*, 341–352. [CrossRef]
15. Boukelia, T.; Arslan, O.; Djimli, S.; Kabar, Y. ORC fluids selection for a bottoming binary geothermal power plant integrated with a CSP plant. *Energy* **2023**, *265*, 126186. [CrossRef]
16. Sun, Q.; Wang, Y.; Cheng, Z.; Wang, J.; Zhao, P.; Dai, Y. Thermodynamic Optimization of a Double-pressure Organic Rankine Cycle Driven by Geothermal Heat Source. *Energy Procedia* **2017**, *129*, 591–598. [CrossRef]
17. Neto, R.d.O.; Sotomonte, C.A.R.; Coronado, C.J. Off-design model of an ORC system for waste heat recovery of an internal combustion engine. *Appl. Therm. Eng.* **2021**, *195*, 117188. [CrossRef]
18. Ping, X.; Yang, F.; Zhang, H.; Xing, C.; Yu, M.; Wang, Y. Investigation and multi-objective optimization of vehicle engine-organic Rankine cycle (ORC) combined system in different driving conditions. *Energy* **2023**, *263*, 125672. [CrossRef]
19. Lee, H.; Ryu, B.; Anh, D.P.; Roh, G.; Lee, S.; Kang, H. Thermodynamic analysis and assessment of novel ORC- DEC integrated PEMFC system for liquid hydrogen fueled ship application. *Int. J. Hydrogen Energy* **2023**, *48*, 3135–3153. [CrossRef]
20. Wang, E.; Zhang, M.; Meng, F.; Zhang, H. Zeotropic working fluid selection for an organic Rankine cycle bottoming with a marine engine. *Energy* **2022**, *243*, 123097. [CrossRef]
21. Yağlı, H.; Koç, Y.; Kalay, H. Optimisation and exergy analysis of an organic Rankine cycle (ORC) used as a bottoming cycle in a cogeneration system producing steam and power. *Sustain. Energy Technol. Assess.* **2021**, *44*, 100985. [CrossRef]
22. Eyerer, S.; Dawo, F.; Wieland, C.; Spliethoff, H. Advanced ORC architecture for geothermal combined heat and power generation. *Energy* **2020**, *205*, 117967. [CrossRef]
23. Pan, M.; Lu, F.; Zhu, Y.; Huang, G.; Yin, J.; Huang, F.; Chen, G.; Chen, Z. Thermodynamic, exergoeconomic and multi-objective optimization analysis of new ORC and heat pump system for waste heat recovery in waste-to-energy combined heat and power plant. *Energy Convers. Manag.* **2020**, *222*, 113200. [CrossRef]
24. Schifflechner, C.; Dawo, F.; Eyerer, S.; Wieland, C.; Spliethoff, H. Thermodynamic comparison of direct supercritical CO_2 and indirect brine-ORC concepts for geothermal combined heat and power generation. *Renew. Energy* **2020**, *161*, 1292–1302. [CrossRef]
25. Lu, X.; Du, B.; Zhu, W.; Yang, Y.; Xie, C.; Tu, Z.; Zhao, B.; Zhang, L.; Song, J.; Deng, Z. Thermodynamic and dynamic analysis of a hybrid PEMFC-ORC combined heat and power (CHP) system. *Energy Convers. Manag.* **2023**, *292*, 117408. [CrossRef]
26. Dinçer, I.; Kanoğlu, M. *Kanoglu, Refrigeration Systems and Applications*, 2nd ed.; John Wiley and Sons, Ltd.: Hoboken, NJ, USA, 2010; ISBN 9780470661093.
27. The Economist Intelligence Unit. *The Cooling Imperative Forecasting the Size and Source of Future Cooling Demand*; Economist Intelligence Unit: London, UK, 2019.
28. Wang, M.; Becker, T.M.; Ferreira, C.A.I. Assessment of vapor–liquid equilibrium models for ionic liquid based working pairs in absorption cycles. *Int. J. Refrig.* **2018**, *87*, 10–25. [CrossRef]
29. Liu, X.; Li, J.; Hou, K.; Wang, S.; He, M. New environment friendly working pairs of dimethyl ether and ionic liquids for absorption refrigeration with high COP. *Int. J. Refrig.* **2022**, *134*, 159–167. [CrossRef]
30. Kallitsis, K.; Koulocheris, V.; Pappa, G.; Voutsas, E. Evaluation of water + imidazolium ionic liquids as working pairs in absorption refrigeration cycles. *Appl. Therm. Eng.* **2023**, *233*, 121201. [CrossRef]
31. Haghbakhsh, R.; Peyrovedin, H.; Raeissi, S.; Duarte, A.R.C.; Shariati, A. Energy Conservation in Absorption Refrigeration Cycles Using DES as a New Generation of Green Absorbents. *Entropy* **2020**, *22*, 409. [CrossRef] [PubMed]
32. Verma, A.; Kaushik, S.C.; Tyagi1, S.K. Performance enhancement of absorption refrigeration systems: An overview. *J. Therm. Eng.* **2023**, *9*, 1100–1113. [CrossRef]
33. Gomri, R. Simulation study on the performance of solar/natural gas absorption cooling chillers. *Energy Convers. Manag.* **2013**, *65*, 675–681. [CrossRef]
34. Shirazi, A.; Pintaldi, S.; White, S.D.; Morrison, G.L.; Rosengarten, G.; Taylor, R.A. Solar-assisted absorption air-conditioning systems in buildings: Control strategies and operational modes. *Appl. Therm. Eng.* **2016**, *92*, 246–260. [CrossRef]
35. Kerme, E.D.; Chafidz, A.; Agboola, O.P.; Orfi, J.; Fakeeha, A.H.; Al-Fatesh, A.S. Energetic and exergetic analysis of solar-powered lithium bromide-water absorption cooling system. *J. Clean. Prod.* **2017**, *151*, 60–73. [CrossRef]
36. Li, N.; Luo, C.; Su, Q. A working pair of $CaCl_2$–LiBr–$LiNO_3$/H_2O and its application in a single-stage solar-driven absorption refrigeration cycle. *Int. J. Refrig.* **2018**, *86*, 1–13. [CrossRef]
37. Ravikumar, T.; Suganthi, L.; Samuel, A.A. Exergy analysis of solar assisted double effect absorption refrigeration system. *Renew. Energy* **1998**, *14*, 55–59. [CrossRef]

38. Babaei, S.M.; Razmi, A.R.; Soltani, M.; Nathwani, J. Quantifying the effect of nanoparticles addition to a hybrid absorption/recompression refrigeration cycle. *J. Clean. Prod.* **2020**, *260*, 121084. [CrossRef]
39. Mohammadi, K.; Jiang, Y.; Borjian, S.; Powell, K. Thermo-economic assessment and optimization of a hybrid triple effect absorption chiller and compressor. *Sustain. Energy Technol. Assess.* **2020**, *38*, 100652. [CrossRef]
40. Goswami, D.Y.; Xu, F. Analysis of a New Thermodynamic Cycle for Combined Power and Cooling Using Low and Mid Temperature Solar Collectors. *J. Sol. Energy Eng.* **1999**, *121*, 91–97. [CrossRef]
41. Leveni, M.; Cozzolino, R. Energy, exergy, and cost comparison of Goswami cycle and cascade organic Rankine cycle/absorption chiller system for geothermal application. *Energy Convers. Manag.* **2021**, *227*, 113598. [CrossRef]
42. Karimi, M.; Dutta, A.; Kaushik, A.; Bansal, H.; Haque, S. A review of organic Rankine, Kalina and Goswami cycle. *Int. J. Eng. Technol. Manag. Appl. Sci.* **2015**, *3*, 90–105.
43. Fontalvo, A.; Pinzon, H.; Duarte, J.; Bula, A.; Quiroga, A.G.; Padilla, R.V. Exergy analysis of a combined power and cooling cycle. *Appl. Therm. Eng.* **2013**, *60*, 164–171. [CrossRef]
44. Rivera, W.; Sánchez-Sánchez, K.; Hernández-Magallanes, J.A.; Jiménez-García, J.C.; Pacheco, A. Modeling of Novel Thermodynamic Cycles to Produce Power and Cooling Simultaneously. *Processes* **2020**, *8*, 320. [CrossRef]
45. Hasan, A.A.; Goswami, D.Y. Exergy Analysis of a Combined Power and Refrigeration Thermodynamic Cycle Driven by a Solar Heat Source. *J. Sol. Energy Eng.* **2003**, *125*, 55–60. [CrossRef]
46. López-Villada, J.; Ayou, D.S.; Bruno, J.C.; Coronas, A. Modelling, simulation and analysis of solar absorption power-cooling systems. *Int. J. Refrig.* **2014**, *39*, 125–136. [CrossRef]
47. Alshammari, S.; Kadam, S.T.; Yu, Z. Assessment of single rotor expander-compressor device in combined organic Rankine cycle (ORC) and vapor compression refrigeration cycle (VCR). *Energy* **2023**, *282*, 128763. [CrossRef]
48. Kim, M.-H. Energy and Exergy Analysis of Solar Organic Rankine Cycle Coupled with Vapor Compression Refrigeration Cycle. *Energies* **2022**, *15*, 5603. [CrossRef]
49. Grauberger, A.; Young, D.; Bandhauer, T. Experimental validation of an organic rankine-vapor compression cooling cycle using low GWP refrigerant R1234ze(E). *Appl. Energy* **2022**, *307*, 118242. [CrossRef]
50. Nasir, M.T.; Ekwonu, M.C.; Esfahani, J.A.; Kim, K.C. Performance assessment and multi-objective optimization of an organic Rankine cycles and vapor compression cycle based combined cooling, heating, and power system. *Sustain. Energy Technol. Assess.* **2021**, *47*, 101457. [CrossRef]
51. Ghorbani, S.; Deymi-Dashtebayaz, M.; Dadpour, D.; Delpisheh, M. Parametric study and optimization of a novel geothermal-driven combined cooling, heating, and power (CCHP) system. *Energy* **2023**, *263*, 126143. [CrossRef]
52. Tao, J.; Wang, H.; Wang, J.; Feng, C. Exergoeconomic and Exergoenvironmental Analysis of a Novel Power and Cooling Cogeneration System Based on Organic Rankine Cycle and Ejector Refrigeration Cycle. *Energies* **2022**, *15*, 7945. [CrossRef]
53. Chowdhury, T.; Mokheimer, E.M.A. Performance Assessment of Solar Parabolic Trough Collector-Assisted Combined Organic Rankine Cycle and Triple Pressure Level Ejector-Absorption Refrigeration Cycle. *J. Energy Resour. Technol.* **2022**, *144*, 4053893. [CrossRef]
54. Liu, Y.; Ding, Y.; Yang, M.; Peng, B.-Y.; Qian, F. A trigeneration application based on compressed air energy storage integrated with organic Rankine cycle and absorption refrigeration: Multi-objective optimisation and energy, exergy and economic analysis. *J. Energy Storage* **2022**, *55*, 105803. [CrossRef]
55. Sharifishourabi, M.; Chadegani, E.A. Performance assessment of a new organic Rankine cycle based multi-generation system integrated with a triple effect absorption system. *Energy Convers. Manag.* **2017**, *150*, 787–799. [CrossRef]
56. Anvari, S.; Saray, R.K.; Bahlouli, K. Conventional and advanced exergetic and exergoeconomic analyses applied to a tri-generation cycle for heat, cold and power production. *Energy* **2015**, *91*, 925–939. [CrossRef]
57. Pashapour, M.; Jafarmadar, S.; Arya, S.K. Exergy Analysis of a Novel Combined System Consisting of a Gas Turbine, an Organic Rankine Cycle and an Absorption Chiller to Produce Power, Heat and Cold. *Int. J. Eng.* **2019**, *32*, 1320–1326. [CrossRef]
58. Jiménez-García, J.C.; Moreno-Cruz, I.; Rivera, W. Modeling of an Organic Rankine Cycle Integrated into a Double-Effect Absorption System for the Simultaneous Production of Power and Cooling. *Processes* **2023**, *11*, 667. [CrossRef]
59. Grosu, L.; Marin, A.; Dobrovicescu, A.; Queiros-Conde, D. Exergy analysis of a solar combined cycle: Organic Rankine cycle and absorption cooling system. *Int. J. Energy Environ. Eng.* **2016**, *7*, 449–459. [CrossRef]
60. Gupta, P.R.; Tiwari, A.K.; Said, Z. Solar organic Rankine cycle and its poly-generation applications—A review. *Sustain. Energy Technol. Assess.* **2022**, *49*, 101732. [CrossRef]
61. NREL. *System Advisor Model, SAM*; NREL: Golden, CO, USA, 2023.
62. Herath, H.; Wijewardane, M.; Ranasinghe, R.; Jayasekera, J. Working fluid selection of Organic Rankine Cycles. *Energy Rep.* **2020**, *6*, 680–686. [CrossRef]
63. Dai, B.; Zhu, K.; Wang, Y.; Sun, Z.; Liu, Z. Evaluation of organic Rankine cycle by using hydrocarbons as working fluids: Advanced exergy and advanced exergoeconomic analyses. *Energy Convers. Manag.* **2019**, *197*, 111876. [CrossRef]
64. Pezzuolo, A.; Benato, A.; Stoppato, A.; Mirandola, A. The ORC-PD: A versatile tool for fluid selection and Organic Rankine Cycle unit design. *Energy* **2016**, *102*, 605–620. [CrossRef]
65. Roy, J.P.; Mishra, M.K.; Misra, A. Performance analysis of an Organic Rankine Cycle with superheating under different heat source temperature conditions. *Appl. Energy* **2011**, *88*, 2995–3004. [CrossRef]

66. Wang, E.H.; Zhang, H.G.; Fan, B.Y.; Ouyang, M.G.; Zhao, Y.; Mu, Q.H. Study of working fluid selection of organic Rankine cycle (ORC) for engine waste heat recovery. *Energy* **2011**, *36*, 3406–3418. [CrossRef]
67. Desai, N.B.; Bandyopadhyay, S. Process integration of organic Rankine cycle. *Energy* **2009**, *34*, 1674–1686. [CrossRef]
68. Maizza, V.; Maizza, A. Unconventional working fluids in organic Rankine-cycles for waste energy recovery systems. *Appl. Therm. Eng.* **2001**, *21*, 381–390. [CrossRef]
69. Wagner, M.J.; Mehos, M.S.; Kearney, D.W.; McMahan, A.C. Modeling of a Parabolic Trough Solar Field for Acceptance Testing: A Case Study. In Proceedings of the ASME 2011 5th International Conference on Energy Sustainability, Washington, DC, USA, 7–10 August 2011; pp. 595–603.
70. Mohammadi, A.; Kasaeian, A.; Pourfayaz, F.; Ahmadi, M.H. Thermodynamic analysis of a combined gas turbine, ORC cycle and absorption refrigeration for a CCHP system. *Appl. Therm. Eng.* **2017**, *111*, 397–406. [CrossRef]
71. Clerx, M.; Trezek, G. Performance of an aqua-ammonia absorption solar refrigerator at sub-freezing evaporator conditions. *Sol. Energy* **1987**, *39*, 379–389. [CrossRef]
72. Merchán, R.; Santos, M.; Medina, A.; Hernández, A.C. High temperature central tower plants for concentrated solar power: 2021 overview. *Renew. Sustain. Energy Rev.* **2022**, *155*, 111828. [CrossRef]